Localized excitations in competing bond-order-wave, charge-density-wave, and spin-density-wave systems

Chui-lin Wang
China Center of Advanced Science and Technology (World Laboratory), P. O. Box 8730, Beijing 100080, China

Wen-zheng Wang, Guo-liang Gu,* and Zhao-bin Su
Institute of Theoretical Physics, Academia Sinica, P. O. Box 2735, Beijing 100080, China

Lu Yu
International Center for Theoretical Physics, P. O. Box 586, Trieste 34100, Italy, and Institute of Theoretical Physics, Academia Sinica, P. O. Box 2735, Beijing 100080, China
(Received 16 November 1992; revised manuscript received 14 May 1993)

The characteristics of localized excitations in quasi-one-dimensional systems are rather sensitive to the interplay between the electron-phonon (e-ph) and electron-electron (e-e) interactions giving rise to competition and possible coexistence of various symmetry-broken ground states such as the bond-order wave (BOW), the charge-density wave (CDW), and the spin-density wave (SDW). Such effects are observable in halogen-bridged mixed-valence transition-metal complexes and can be elucidated within the Bogoliubov–de Gennes formalism using an extended Peierls-Hubbard model. The coexistence of local BOW, CDW, and SDW distortions is demonstrated in this paper for polarons and self-trapped excitons (STE) in different symmetry-broken ground states. An extensive study of localized excitations over a wide range of the on-site e-ph coupling λ_2 and the Hubbard interaction U leads to the following observations. (a) As λ_2 increases at fixed U, the number of bound states inside the gap changes from two to four for the STE case and from two to three for the polaron case. (b) Upon its further increase, one type of STE with a certain pattern of SDW distortion and charge transfer is transforming into another type of STE with a different pattern. (c) A nonmonotonic dependence of the lattice relaxation energy on λ_2 is predicted within the lattice relaxation approach developed by Su and Yu earlier, and is attributed to a crossover from the weak-coupling to strong-coupling behavior showing up as the emergence of new bound states inside the gap. Moreover, the nonradiative transition rate of STE is also calculated and is used to tentatively interpret the very short lifetime of STE in PtCl complexes. Such nonmonotonic dependence of the relaxation rate on the coupling constant may also be observed in other quasi-one-dimensional systems as well.

I. INTRODUCTION

For the last two decades the experimental and theoretical studies of quasi-one-dimensional systems, like conducting polymers, charge-transfer solids (e.g., TTF-TCNQ), charge-density-wave systems (e.g., $NbSe_3$), and halogen-bridged mixed-valence, transition-metal linear-chain complexes (HMMC or MX chains) have attracted great interest among physicists and chemists. Apart from potential applications, the scientific motivation is mainly due to the availability of a variety of symmetry broken ground states like BOW, CDW, SDW, and the spin-Peierls state, their competition and possible coexistence determined by the interplay between the electron-electron (e-e) and electron-phonon (e-ph) interactions. Even more interesting are the localized excitations such as solitons, polarons, bipolarons, and excitons on these ground states and their contributions to various observable effects like optical absorption and resonance Raman scattering. Among these quasi-one-dimensional systems, the MX chains are of particular interest because members of this family share the same crystalline structure, while their physical properties depend strongly on the species and structures of the constituent metal (M) or halogen (X) ions, and also on the organic ligands (L) and counter ions (X or ClO_4^-). By "tuning " the strengths of e-e and e-ph couplings, a big variety of states ranging from SDW (e.g., NiBr), weakly distorted CDW (e.g., PtI) to strongly coupled CDW (e.g., PtCl) can be materialized. Therefore, these compounds are ideal prototypes for the study of competing BOW, CDW, and SDW states, which is evidenced by the large amount of experimental and theoretical investigations devoted to them.[1–3]

From the theoretical point of view, the phase diagram of these compounds has been studied within the extended Peierls-Hubbard model by Nasu,[4] while the mapping of the MX chains with on-site e-ph coupling and Hubbard repulsion onto the Su-Schrieffer-Heeger (SSH) model of polyacetylene[5] and the existence of solitons were considered by Ichinose.[6] The weak coupling continuum model was studied by Onodera,[7] whereas the strong coupling limit with competing BOW and CDW order was investigated by Baeriswyl and Bishop.[8] Furthermore, Bishop, Gammel, and Phillpot have proposed a two-band model[9]

to describe various physical properties of the MX chains and an extensive series of studies have been carried out using this model.[10] The physical parameters involved in these models can be determined either from the band structure calculations[11] or from the valence-bond calculations on small clusters.[12]

In this paper, we focus on the localized excitations in the competing BOW, CDW, and SDW systems, paying special attention to their dependence on the coupling strength, since the salient tunability of the MX-chain family in practice spans a wide scope of realistic parameters. We find that the characteristics of localized excitations are rather sensitive to the interplay between the e-e and e-ph interactions. We have explored various parts of the phase diagram, including both BOW-CDW and CDW-SDW competitions, and have studied in particular detail the dependence of localized excitations on the on-site e-ph coupling λ_2 and the Hubbard U in the CDW dominating regime. In order to simplify the issue and to emphasize the main physical features of the effects under discussion, we use a simple one-band model instead of the more realistic, but more complicated two-band model proposed by Bishop, Gammel, and Phillpot.[9] It is reasonable to expect that the main effects we describe here will survive in the two-band case as well. During this research work we have found the following.

(1) As to homogeneous states, they may coexist (like BOW and CDW) or exclude each other (like SDW and CDW without BOW), but the local distortions of the order parameters can always coexist, only subject to the symmetry requirements of the problem. For example, a BOW kink will be accompanied by a CDW polaron, and vice versa. Similarly, a self-trapped exciton (STE) in the CDW dominating regime will contain local SDW distortion and vice versa. This effect has been observed in studies on polyacetylene,[13] MX chains,[10,14,15] and in cuprate superconductors.[16] However, we would like to emphasize this effect and carefully examine its implications.

(2) As a conventional wisdom one would expect that the relaxation rate of localized excitations will be a monotonic function of the coupling strength. However, we have found a counterexample showing nonmonotonicity. This is mainly due to a crossover from the weak-coupling to strong-coupling behavior signalled by the emergence of new bound states inside the energy gap at a certain value of the coupling strength. It will give rise to observable effects.

(3) It is natural to think that the localized excitations of a given type, say STE in a CDW dominating region, would have the same character and pattern as the coupling strength changes. However, this is not true either. There is a well defined boundary in the parameter space where one pattern of excitation is converted into another pattern, both being compatible with the symmetry requirements. This effect should also have observable consequences.

In view of difficulties in finding analytic solutions of the problem, most of our studies were performed numerically using the self-consistent Bogoliubov–de Gennes (BdeG) formalism.[17] The Hartree-Fock (HF) eigenequations are first solved for a given lattice configuration, and then the final stable lattice configuration is determined self-consistently through the gap equations obtained by minimizing the total energy of the system. In order to rule out the finite size effects, the number of sites in the chain has been varied from 20 to 200, and consistent results have been obtained with a precision better than 10^{-6}. Of course, it is not trivial to judge numerically whether a state is localized or not. In our calculations, we first examined the correlation length [roughly the half-width of the localized configuration and the corresponding highest occupied molecular orbital (HOMO) wave function] which should be much less than the chain size and should be independent of its change, then checked the possible additional bound states whose energy level should be separated from the continuum band, and whose wave function should be localized in comparison with the extended band states. Special caution should be taken in interpreting results of a finite size calculation in the weak coupling limit where the extent of excitations would diverge. In this case results of the continuum model should be quoted as a reference. In order to avoid the topological defects, only even-membered chains have been considered.

The rest of the paper is organized as follows. In the next section, we first describe the model Hamiltonian and its symmetry properties, and then briefly review the ground state properties and illustrate the CDW-SDW competition phase diagram, derived by the BdeG formalism, as a guideline to the succeeding calculations. In Sec. III, the configurations and electronic structures of polarons and STE are demonstrated in various subsections corresponding to the competitions of BOW-CDW and CDW-SDW, respectively. The coexistence of local BOW-CDW and CDW-SDW distortions is clearly shown. As main consequences of varying the driving on-site e-ph coupling λ_2 and e-e interaction U, the emergence of new bound states and the crossover of STE types are elucidated in detail. The attendant nonmonotonic dependence of the lattice relaxation energy due to the emergence of new bound states and its implication for the nonradiative transition process of STE are manifested in Sec. IV. Finally, in Sec. V, the calculated nonradiative transition rate is used to interpret the very short lifetime for STE in PtCl materials. Other possible experimental consequences are also discussed. The details of the lattice relaxation formalism are summerized in Appendix A, while the calculation of the multielectron matrix elements is outlined in Appendix B to make this paper more self-contained. Brief reports on some obtained results have appeared earlier.[18,19]

II. GROUND STATE PROPERTIES

A. The model Hamiltonian and its symmetry

In the context of conducting polymers,[17] the one-dimensional Peierls-Hubbard Hamiltonian provides a theoretical framework capable of treating both e-ph and e-e interactions, and has been successful in interpreting various experiments. The model for the MX chain systems is written as[4,8]

$$H = -\sum_{i,s}[t_0 - \alpha(u_{i+1} - u_i)](c^\dagger_{i+1\,s}c_{i\,s} + \text{H.c.}) - \sum_{i,s}\beta(v_{i+1} - v_i)c^\dagger_{i\,s}c_{i\,s}$$
$$+U\sum_i n_{i\uparrow}n_{i\downarrow} + V\sum_{i,s,s'} n_{i\,s}n_{i+1\,s'} + \frac{K}{2}\sum_i[(u_i - v_i)^2 + (u_i - v_{i+1})^2], \tag{2.1}$$

where $c^\dagger_{i\,s}$ ($c_{i\,s}$) creates (annihilates) an electron in the d_{z^2} orbital of the M (metal) ion at site i with spin s. It is assumed that each metal ion in the MX chain contributes an unpaired electron, which can supertransfer between the d_{z^2} orbitals of neighboring M atoms bridged by the X ions forming a charge-transfer band, where t_0 is the supertransfer energy (hopping integral) between M ions. The total number of such electrons N is equal to the total number of M ions in the ground state. v_i and u_i are static displacement coordinates for the ith X (halogen) ion and M ion, respectively; β and α are the intrasite and inter-site e-ph coupling constants, which describe the couplings of electrons to two different phonon modes. The charge transfer rate is determined by the resonance integral, i.e., $t_0 - \alpha(u_{i+1} - u_i)$. The on-site energy of the electron depends on the distance between neighboring X ions as $-\beta(v_{i+1} - v_i)$ in the tight-binding picture. U and V denote the on-site and nearest-neighbor Coulomb interactions between electrons, respectively. K is the stiffness constant, and the kinetic energy of ions is neglected here for our quasistatic calculations, while effects due to quantum fluctuations of phonons are another topic for further considerations. This Hamiltonian exhibits obvious competition between the Peierls instability coming from the intrasite e-ph coupling (β-term) producing CDW, and the intersite e-ph coupling (α-term) yielding BOW, and the Hubbard instability coming from the e-e correlations (U and V terms) giving rise to the magnetic SDW. It is convenient to introduce dimensionless parameters

$$\lambda_1 = \frac{4\alpha^2}{\pi K t_0}, \qquad \lambda_2 = \frac{\beta^2}{\pi K t_0},$$
$$\delta_i = (-1)^{i+1}\frac{2\alpha u_i}{t_0}, \qquad \gamma_i = (-1)^{i+1}\frac{\beta v_i}{t_0}, \tag{2.2}$$

and to measure energy in units of t_0, i.e., $H/t_0 \longrightarrow H$, $U/t_0 \longrightarrow U$, $V/t_0 \longrightarrow V$.

Moreover, the intrasite e-ph coupling (β-term) spoils the single-particle charge conjugation symmetry possessed by the SSH model,[8,17] and produces important consequence, *e.g.*, the single electron energy levels of this system are no longer symmetrically distributed around zero for a general configuration and coupling strength. Of course, this asymmetry persists in the two-band model.[9] Nevertheless, several combined symmetries can be found in this situation. It can be easily shown that the Hamiltonian (2.1) is invariant under the following symmetry operations:

$$\begin{cases}\gamma_i \longrightarrow \gamma_{-(i-1)}\\ \delta_i \longrightarrow -\delta_{-i}\\ c_{is} \longrightarrow c_{-i\bar{s}}\end{cases} \text{or} \quad \begin{cases}\gamma_i \longrightarrow \gamma_{-(i-1)}\\ \delta_i \longrightarrow -\delta_{-i}\\ c_{is} \longrightarrow c_{-is}\end{cases}, \tag{2.3}$$

$$\begin{cases}\gamma_i \longrightarrow -\gamma_{-i}\\ \delta_i \longrightarrow \delta_{-(i+1)}\\ c_{is} \longrightarrow c_{-(i+1)\bar{s}}\end{cases} \text{or} \quad \begin{cases}\gamma_i \longrightarrow -\gamma_{-i}\\ \delta_i \longrightarrow \delta_{-(i+1)}\\ c_{is} \longrightarrow c_{-(i+1)s}\end{cases}, \tag{2.4}$$

where $\bar{s}$ means spin orientation opposite to s. These are combined parity and translation symmetry operations, which hold for any electron filling and any excitations. Particularly, for $\lambda_1 = 0$ and the half-filling case, two other kinds of symmetry operations hold for periodic boundary conditions, namely

$$\begin{cases}\gamma_i \longrightarrow \gamma_{-i}\\ c_{is} \longrightarrow (-)^i c^\dagger_{-(i+1)s}\end{cases} \text{or} \quad \begin{cases}\gamma_i \longrightarrow \gamma_{-i}\\ c_{is} \longrightarrow (-)^i c^\dagger_{-(i+1)\bar{s}},\end{cases} \tag{2.5}$$

$$\begin{cases}\gamma_i \longrightarrow -\gamma_{-(i-1)}\\ c_{is} \longrightarrow (-)^i c^\dagger_{-is}\end{cases} \text{or} \quad \begin{cases}\gamma_i \longrightarrow -\gamma_{-(i-1)}\\ c_{is} \longrightarrow (-)^i c^\dagger_{-i\bar{s}}.\end{cases} \tag{2.6}$$

These are generalized electron-hole symmetries which combine parity, translation, and charge conjugation operations. It is noted that the CDW lattice distortions γ_i and BOW lattice distortions δ_i are of opposite parity in Eqs. (2.3) and (2.4), and they possess different symmetry centers. Therefore, the CDW order parameter $\langle n_{i\uparrow}\rangle + \langle n_{i\downarrow}\rangle - 1$ (1 is the average density of electrons in the system) and the SDW order parameter $\langle n_{i\uparrow}\rangle - \langle n_{i\downarrow}\rangle$ may have different parity and symmetry centers. For example, the second set of Eq. (2.3) shows even parity of γ_i, CDW, and SDW order parameters, and odd parity of δ_i; while the first set of Eq. (2.5) gives odd CDW, SDW order parameters, and even γ_i. The consequences for the stability of various exciton and polaron solutions obeying different symmetries will be discussed in Sec. III.

B. Phase diagrams

The homogeneous ground state properties of such a system ($\delta_i = \delta_0$, $\gamma_i = \gamma_0$) have been extensively studied in Ref. 8 with $U = V = 0$, and in Refs. 4 and 19 with $U \neq 0, V \neq 0$. Baeriswyl and Bishop[8] indicated that the intrasite and intersite e-ph couplings lead to a competition between the CDW and BOW ground states, and there are three regions in the competing BOW-CDW phase diagram where the λ_2 dominating region [$\lambda_2 > \lambda_1/(1 + 2\lambda_1)$] corresponds to CDW states

with $\delta_0 = 0$, $\gamma_0 \neq 0$, and the λ_1 dominating region $[\lambda_2 < \lambda_1/(1 + 2\lambda_1)]$ prefers a BOW order with $\delta_0 \neq 0$, $\gamma_0 = 0$, while the small intermediate region near the phase boundary $\lambda_2 = \lambda_1/(1 + 2\lambda_1)$ corresponds to coexistence of CDW and BOW states with $\delta_0 \neq 0$, $\gamma_0 \neq 0$. We will use their phase diagram in guiding our numerical studies on localized excitations in the BOW-CDW competition regime. On the other hand, as U and V are included, it has been shown analytically by Nasu[4] and numerically through the BdeG formalism[19] that the dominance of U leads to a SDW state, while the CDW state prevails in the λ_2 dominating region, and that homogeneous CDW and SDW states cannot coexist without involving BOW.

In order to define the parameter regions for the succeeding analysis of localized excitations, the CDW-SDW phase diagram, obtained by the BdeG formalism,[19] is shown in Fig. 1, where the parameter space is divided into three main characteristic zones. In zone-I (above curve OF) corresponding to large U and the small λ_2 region, the SDW states dominate, and the CDW state cannot be found there, i.e., this is a pure SDW region where both the CDW order parameter and γ vanish. Oppositely, zone-III (below curve OE), is a pure CDW region where γ and the CDW order parameter increase with λ_2, while the SDW order parameters vanish. Interestingly, the intermediate region, i.e., zone-II, where the competition of CDW and SDW is taking place, can be divided into two subzones: zone-II(1) and zone-II(2). We notice that unlike the case of the SSH model for polyacetylene,[5]

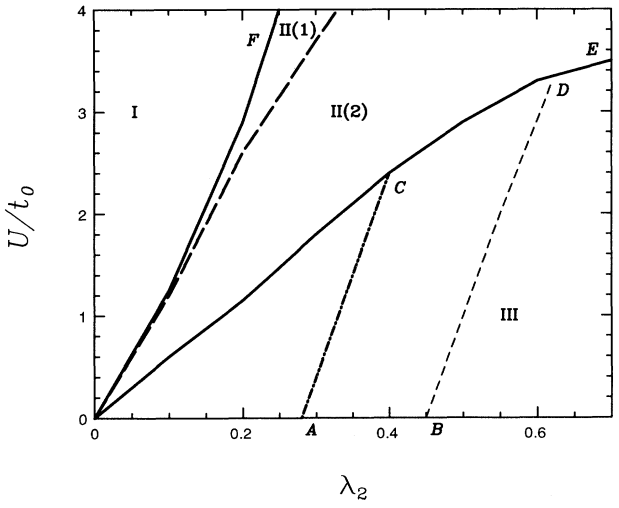

FIG. 1. Phase diagram of the model system. For the homogeneous ground states, zone-I and zone-III correspond to a pure SDW region and a pure CDW region, respectively, while zone-II corresponds to the intermediate region where the competition of CDW and SDW states is found. In zone-II(1) and zone-II(2), SDW and CDW are the most stable solutions, respectively. For the excitonic states, curve AC indicates the crossover from a two-bound-states region (left) to the four-bound-states region (right), while curve BD shows the crossover from the type-I STE region (left, see Fig. 8) to the type-II STE region (right, see Fig. 9).

the energy curve at $\gamma = 0$ no longer shows a local maximum, but rather a local minimum corresponding to a metastable SDW state. In zone-II(1), the $\gamma = 0$ SDW state corresponds to a true ground state, while the doubly degenerate CDW states are metastable. To the contrary, in zone-II(2), the two degenerate CDW states correspond to the ground state, whereas the SDW state is metastable. The meaning of lines AC and BD will be explained in the next section.

III. LOCALIZED EXCITATIONS

Various inhomogeneous excitations have been obtained by Baeriswyl and Bishop[8] in the limit of strong on-site e-ph coupling λ_2, i.e., $\lambda_2 \longrightarrow \infty$ as $t_0 \longrightarrow 0$, while the continuum limit of this model[7] has been discussed in the limit of small λ_1 and λ_2. The lack of analytical solutions of the Hamiltonian (2.1) (even in the absence of U and V) except in the limits mentioned above prompts us to study it numerically in a wide parameter range within the site-dependent mean field theory, i.e., the BdeG formalism. Some related results were obtained earlier by Mishima and Nasu.[14] In this section, we demonstrate systematically the configurations and electronic structures of polarons and STE in different regimes of competing BOW-CDW and CDW-SDW systems. For clarity and simplicity, under the BOW-CDW and CDW-SDW competitions, the e-e interaction U and the intersite e-ph coupling λ_1 are set to zero, respectively. Effects of these neglected terms will be discussed in Sec. V.

A. Polarons under BOW-CDW competition

In this subsection we consider polarons in competing BOW-CDW systems neglecting the Coulomb interactions.

In the adiabatic limit, an electron-polaron is generated after one electron is added to the bottom of the conduction band, while the lattice distortions are introduced in a general form as in the literature of polyacetylene[17] to trigger the localized excitations. As mentioned in the Introduction, within the BdeG formalism, the HF eigenequations of Hamiltonian (2.1) are first solved for a given configuration, then the minimization of the total energy is materialized by solving the two gap equations for δ_i and γ_i to update the configurations until the self-consistency is obtained. One typical solution of electron-polarons in the CDW dominating region (i.e., the λ_2 dominating region in the phase diagram) is shown in Fig. 2(a). In the self-trapping process, a polaron of the order parameter γ_i in the CDW channel emerges from the CDW ground state $\gamma_i = \gamma_0$, whereas the BOW order parameter δ_i transforms from $\delta_i = 0$ into a kinklike configuration in the central part of the chain. Likewise, in the BOW dominating region (i.e., the λ_1 dominating region in the phase diagram), a kinklike configuration can be generated in the CDW channel during the formation of a BOW polaron, as shown in Fig. 2(b). There are also localized SDW distortions accompanying the polaron

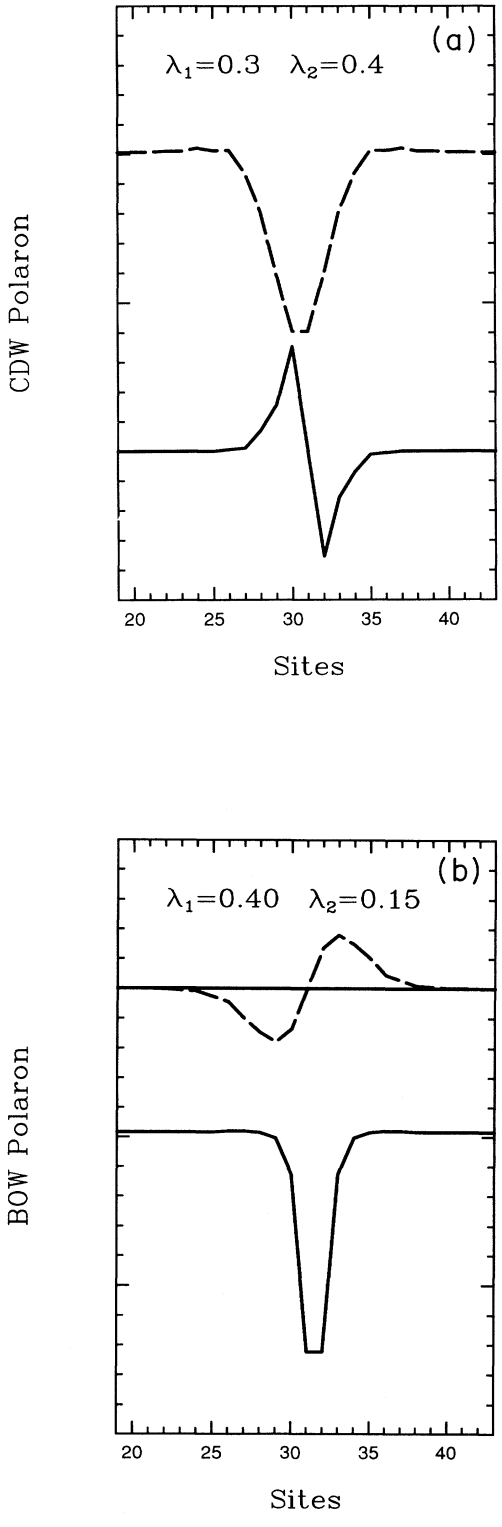

FIG. 2. The configuration of an electron-polaron in (a) the CDW region, (b) the BOW region. A polaron of the order parameter γ_n (dashed) is accompanied by a kink of the order parameter δ_n (solid) in (a), and vice versa in (b). Here γ_n and δ_n satisfy the first set of symmetry relations in Eq. (2.3). $U = V = 0.0$.

even in the absence of the e-e interaction. A similar phenomenon has been observed in the two-band model.[10] It is noted that the polaron configuration satisfies the first set of symmetry relations in Eq. (2.3), where the CDW and BOW order parameter γ_i and δ_i are of even and odd parity, respectively. It is this symmetry requirement that excludes the possibility of forming polarons in both CDW and BOW channels simultaneously.

The intragap levels of the CDW polaron (i.e., the λ_1 dominating region) as a function of λ_2 at fixed $\lambda_1 = 0.3$ are shown in Fig. 3, while these levels as functions of λ_1 at fixed $\lambda_2 = 0.4$ are shown in Fig. 4. In Fig. 3, there are two bound states inside the gap when the intrasite e-ph coupling strength λ_2 is below 0.34, but as λ_2 is increased beyond this critical value, a new bound state splits from the top of the valence band. As seen in Fig. 4, there are three bound states within the gap, even if the intersite e-ph coupling strength λ_1 is zero, which indicates that the emergence of new bound states is mainly caused by the strength of the intrasite e-ph coupling λ_2. As will be shown in Sec. III C, a similar situation also occurs for STE and it will have important physical consequences. It is also noticed that the CDW gap does not vary with λ_1 (see Fig. 4), but it does increase with λ_2 (see Fig. 3). On the other hand, the intragap levels vary with both parameters. The two figures also show the asymmetry of the gap levels with respect to the midgap, which reflects violation of the single-particle electron-hole symmetry due to the presence of λ_2.

B. Polarons under CDW-SDW competition

In this subsection we consider polarons in competing CDW-SDW systems, neglecting the intersite e-ph interaction λ_1.

Under the CDW-SDW competition, the inhomogeneous excitations in the polaron channel are evaluated in zone-III and zone-II of Fig. 1, and the results on the hole-polaron and electron-polaron in zone-III are shown in Figs. 5(a) and 5(b), respectively. The configurations of polarons contain locally nonvanishing SDW distortions in the CDW dominating regime, zone-III and zone-II(2), and nonvanishing CDW distortions in the SDW dominating regime, zone-II(1). It is noted that the polaron solutions can only satisfy the symmetries in Eq. (2.3) or Eq. (2.4) for doping with electrons and holes, respectively. The center of the electron-polaron is shifted by one M-M distance compared with that of the hole-polaron because a hole-polaron favors an oxidized M ion in the CDW ground state while an electron-polaron energetically prefers to reside on a reduced M ion, although they are of about the same size. The creation energy of the electron-polaron is larger than that of the hole-polaron due to the effects of e-e interaction U. There are three bound states as the e-ph coupling λ_2 is increased beyond or the Hubbard U is decreased below some critical values.[19] It is also noted that in the case of nonvanishing nearest neighbor Coulomb interaction V, it does not modify the above results substantially, if V is small compared with U and t_0.

C. STE under CDW-SDW competition

In this subsection we study STE in various regions of the phase diagram (Fig. 1), exhibiting the CDW-SDW competition.

Unlike the case of polyacetylene,[17] the energy of STE in the MX-chain systems is not degenerate with that of a soliton-antisoliton pair even in the absence of Coulomb interactions. Therefore, STE is a rather stable excitation playing an important role in the actual optical processes.[20,21] At the strong coupling limit ($\lambda_2 \to \infty$, $t_0 \to 0$, and $\lambda_1 = 0$, $U = V = 0$), the analytical configuration of STE has been given in Ref. 8. However, as will be shown in this subsection, the presence of finite t_0 and U will give rise to rather substantial modifications of the STE structure. In the adiabatic limit, one electron at the top of the valence band is initially photoexcited to the bottom of the conduction band, with one hole left at the top of the valence band. After the relaxation process, the system will finally reach a stable state with localized lattice distortions and the attendant single electronic states split from the continuum band. The numerical procedure is the same as described before, while the lattice distortions are given by the self-consistent solutions of the gap equations j

$$\gamma_n = (-)^{n+1}\frac{\pi\lambda_2}{2}\sum_{k,s}[\ \psi^2_{ks}(n) - \psi^2_{ks}(n-1)\ ]\ , \qquad (3.1)$$

where ψ_{ks} are the eigenfunctions of Hamiltonian (2.1), and the summation is taken over the occupied states only.

First consider the CDW region without Coulomb interactions (i.e., along the x axis in Fig. 1), where the effect of the on-site e-ph coupling λ_2 on the lattice distortions γ_i of STE is manifested in Fig. 6. For the weak coupling case the lattice distortion is small, but there is a sizable fraction of chain with reversed distortion, like a soliton-antisoliton pair. On the other hand, in the strong coupling limit γ_i is large, and strongly localized, but the reversed distortion is almost absent. Correspondingly, the gap levels of STE as functions of λ_2 are plotted in Fig. 7. As expected, the energy gap increases with the increase of the coupling constant λ_2. When one electron is excited from the valence band to the conduction band, two localized bound states near the midgap are split off from the top of the valence band and the bottom of the conduction band in the weak coupling range. Each of these two bound states is occupied by one electron. As the coupling constant λ_2 increases to around $\lambda_2 = 0.28$, two *new* bound states emerge out from the continuum resulting in a total of four localized bound states inside the gap. The new lower bound state is occupied by two electrons whereas the upper one is empty. These two new bound states play an important role in the calculation of the lattice relaxation rate as will be shown in Sec. IV. As λ_2 increases further, no more new bound states split off from the continuum. This feature has been indicated by Baeriswyl and Bishop[8] in the strong coupling

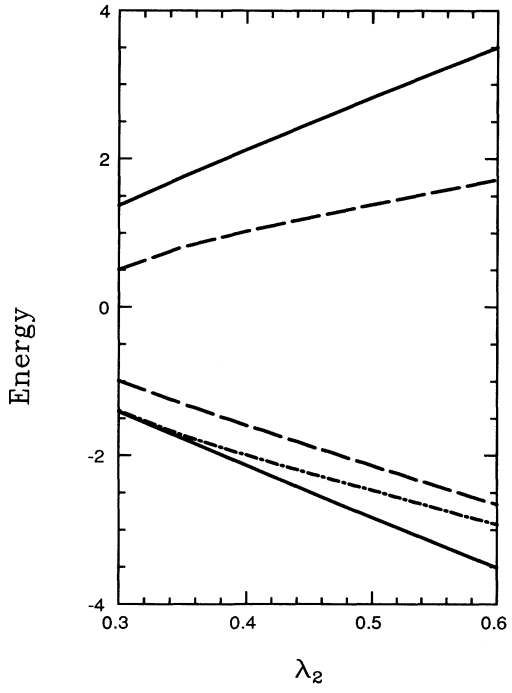

FIG. 3. Intragap levels of the electron-polaron under the BOW-CDW competition between the band edges (solid) in the CDW region as a function of the intrasite e-ph coupling strength λ_2, where $\lambda_1 = 0.3$, $U = V = 0.0$.

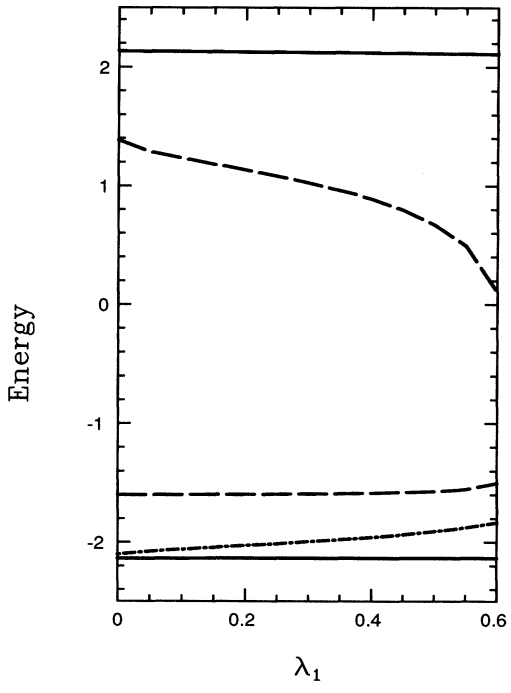

FIG. 4. Intragap levels of the electron-polaron under the BOW-CDW competition between the band edges (solid) in the CDW region as a function of the intersite e-ph coupling strength λ_1, where $\lambda_2 = 0.4$, $U = V = 0.0$.

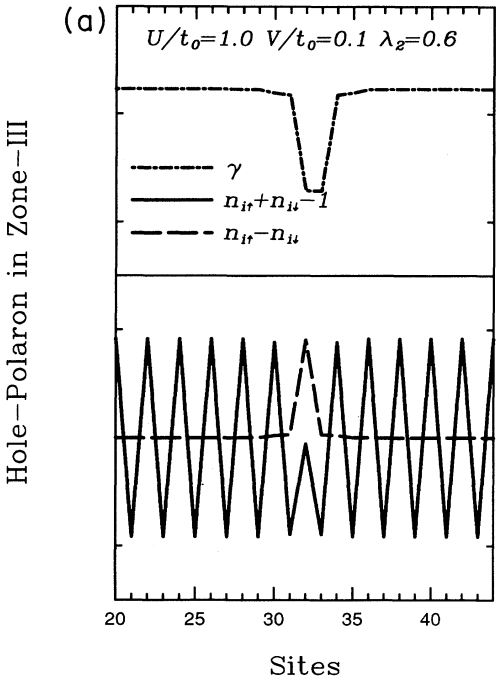

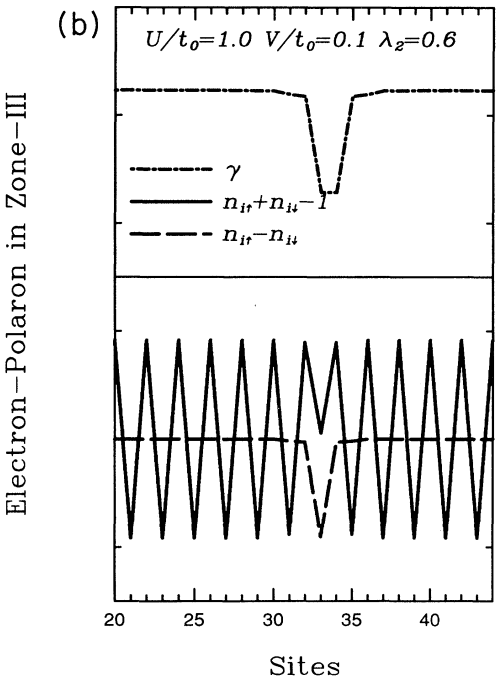

FIG. 5. The configuration of (a) hole-polaron; (b) electron-polaron in zone-III of Fig. 1 under CDW-SDW competition. $U = 1.0$, $V = 0.1$, $\lambda_2 = 0.6$, $N = 64$, which contains nonvanishing localized SDW distortions and satisfies the symmetry relations of Eq. (2.3). Only the configuration near the defect is shown in the figure.

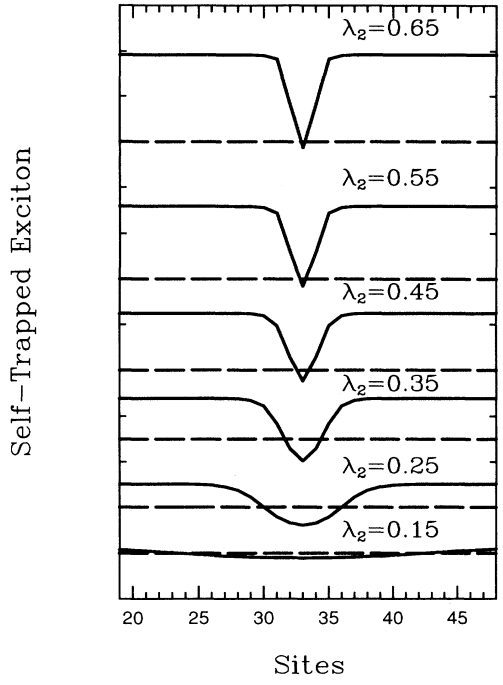

FIG. 6. The configurations of STE in the pure CDW region (along the x axis in Fig. 1) with increasing e-ph coupling λ_2, where γ_n (solid) satisfy the first set of symmetry relations in Eq. (2.4). $\lambda_1 = 0.0$, $U = V = 0.0$.

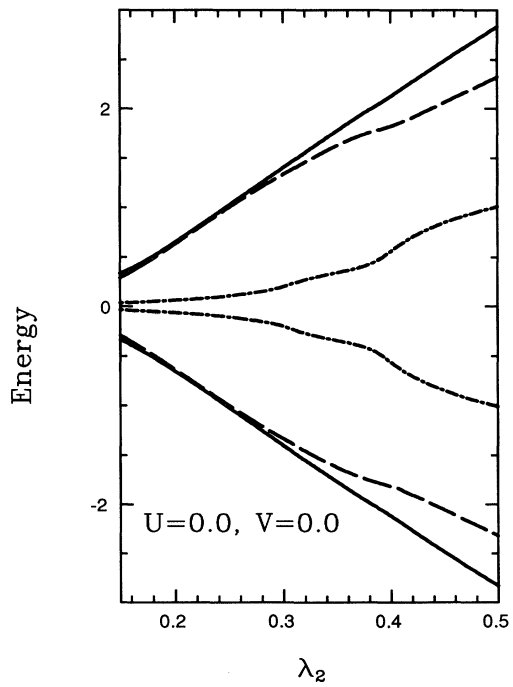

FIG. 7. Intragap levels of STE corresponding to the configuration in Fig. 6 between the band edges (solid) as a function of λ_2, $\lambda_1 = 0.0$, $U = V = 0.0$.

limit, $\lambda_2 \longrightarrow \infty$, where they found only four localized bound states associated with a tightly bound exciton, and the corresponding energy levels are $\epsilon_{\pm 1} = \pm\frac{1}{4}\Delta$, and $\epsilon_{\pm 2} = \pm\frac{3}{4}\Delta$, respectively. The exciton creation energy is $E_{\rm ex} = \frac{5}{4}\Delta$, where Δ is the gap parameter. To study the influence of the finite size effects, we have calculated the exciton configuration for different numbers of chain sites. For chain sites $N = 32$, 64, and 128, no substantial differences have been found in plotting Fig. 6 and Fig. 7. Thus the possibility that the change of bound state number is due to the finite size effects is ruled out. As in the polaron case, the intrasite e-ph coupling λ_2 is the major factor leading to the emergence of new bound states even if λ_1 is included.

As the Hubbard interaction is included, the main features of STE are indicated in Fig. 1. In zone-I, as expected, no localized excitations (neither excitons nor polarons) are found since the localized distortions of γ_i are so tiny compared with the electronic kinetic energy that no self-trapping is taking place. On the contrary, STE can be easily found in zone-III, where the ground state is purely of CDW character. However, the local SDW order parameter does not vanish within the localized STE. One type of STE configuration is shown in Fig. 8, where the localized SDW distortion is clearly seen. When parameters U and λ_2 cross the curve AC in Fig. 1, the number of intragap bound states changes from two to four. Moreover, when parameter values cross the curve BD (with λ_2 increased and/or U decreased), one type of STE with a certain pattern of SDW distortions is transforming into another type of STE with a different pattern. For type-I STE (see Fig. 8), the SDW order parameter behaves like a localized SDW distortion, and the charge transfer from the CDW ground state takes place in both directions within a range of about eight sites. However, for type-II STE (see Fig. 9), the SDW order parameter behaves like a spin kink, where the sign of spin density on the left side of the symmetry center is opposite to that of the right side, while the charge transfer takes place only on the right side within a range of about four sites. Both types of STE's satisfy the first set of symmetry relations in Eq. (2.5), where the CDW and SDW order parameters are odd functions of the chain coordinates, while the lattice distortions γ_i are of even parity. There are other types of STE which satisfy other symmetries. However, their creation energies are all higher than the above solutions according to our calculations.

In zone-II(1), no stable STE with only localized SDW distortions can be found because of the dominance of SDW in the ground state, but solutions of STE with localized CDW distortions, satisfying the first set of symmetry relations in Eq. (2.5), have been found. One ex-

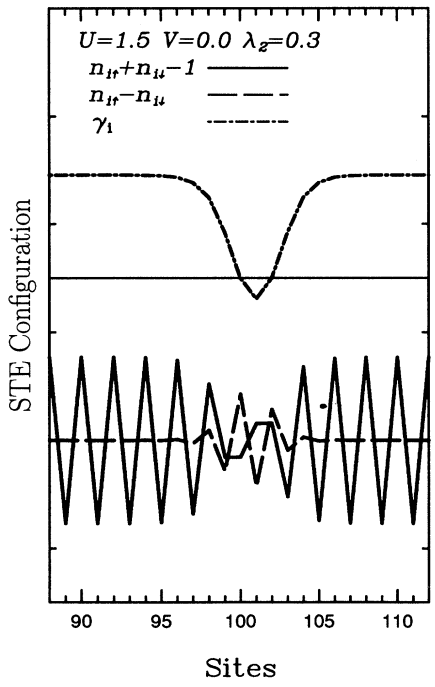

FIG. 8. The configuration of type-I STE on the left of line BD in zone-III of Fig. 1, $U = 1.5$, $V = 0.0$, $\lambda_2 = 0.3$, $N = 200$, where the SDW order parameter behaves like a well-localized spin-density wave, while the charge transfer about eight sites. This type of STE satisfies the first set of symmetry relations in Eq. (2.5). Only the configuration near the STE is shown in the figure.

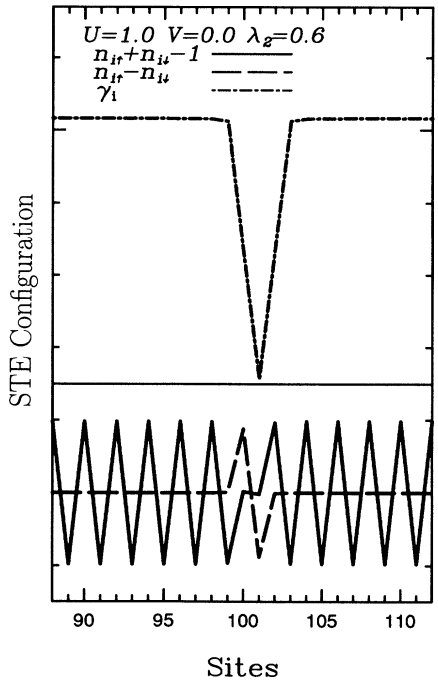

FIG. 9. The configuration of type-II STE on the right of line BD in zone-III of Fig. 1, $U = 1.0$, $V = 0.0$, $\lambda_2 = 0.6$, $N = 200$, where the SDW order parameter behaves like a spin-kink, in which the sign of spin densities in the left side of the symmetry center is contrary to that of the right side, while the charge transfer takes place only on the right side in a range of about four sites. This type of STE also satisfies the first set of symmetry relations in Eq. (2.5). Only the configuration near the STE is shown in the figure.

ample is shown in Fig. 10 for a set of typical parameters. The situation in zone-II(2) is more complicated than zone-III because of rearrangements of energy levels for two different spin orientations due to the stronger e-e interaction U compared with zone-III. Therefore, several solutions satisfying different symmetries are possible in this regime, from which we can determine the solution with the lowest excitation energy for a given set of physical parameters. For example, in the situation shown in Fig. 11, the lowest STE satisfies the symmetry relations in Eq. (2.3), in which all three order parameters are of even parity. It is worthwhile to notice again that the on-site e-ph coupling λ_2 is the major driving factor for the crossover of STE types since the position of point B in Fig. 1 indicates that this crossover still exists even if U is absent.

The structure of the electronic energy levels is shown in Fig. 12, for a fixed λ_2 and varying U. It is noted that unlike the CDW case in the absence of Coulomb interactions (Fig. 7), the energy levels for different spin orientations split due to the e-e interaction U, which is believed to be one of the main reasons for the occurrence of inhomogeneous structures of the SDW and CDW order parameters. Also, the number of bound states inside the gap depends on U and λ_2. The regions of different bound state numbers are divided by curve AC in Fig. 1, where the left side corresponds to the region with two localized bound states for each spin orientation, while the right side corresponds to the region with four bound states. It is interesting to notice in Fig. 1 that for $0.28 < \lambda_2 < 0.4$

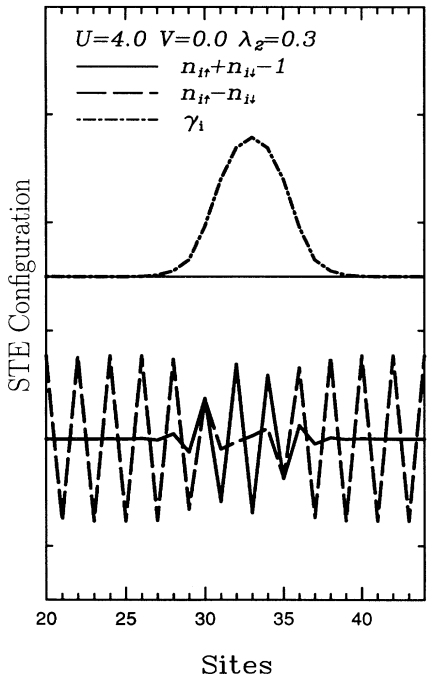

FIG. 10. The configuration of STE in zone-II(1) of Fig. 1, $U = 4.0$, $V = 0.0$, $\lambda_2 = 0.3$, $N = 64$, which possesses localized CDW distortions and satisfies the symmetry relations in Eq. (2.5). Only the configuration near the STE is shown in the figure.

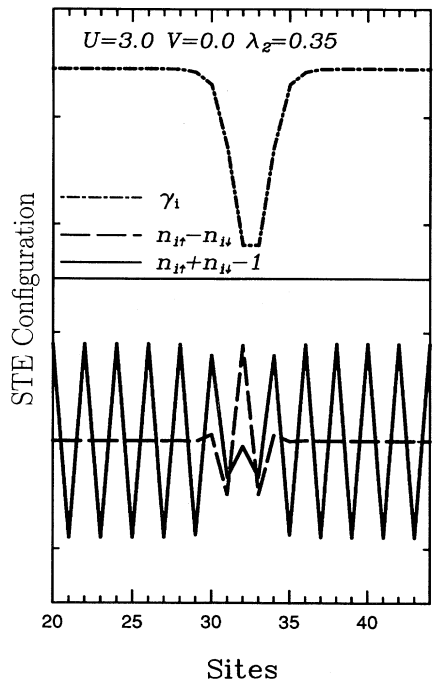

FIG. 11. The configuration of STE in zone-II(2) of Fig. 1, $U = 3.0$, $V = 0.0$, $\lambda_2 = 0.35$, $N = 64$, which is the lowest energy STE possessing localized SDW distortions with this set of parameters and satisfying the symmetry of Eq. (2.3). Only the configuration near the STE is shown in the figure.

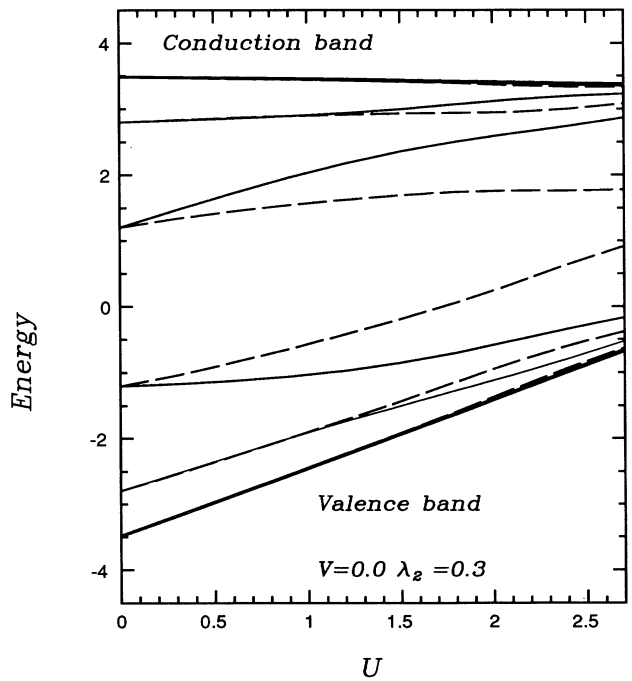

FIG. 12. The energy levels of STE in zone-III and zone-II(2) of Fig. 1 as functions of U. $V = 0.0$, $\lambda_2 = 0.3$, $N = 64$. Only a few levels near the gap edge are shown in the figure.

the number of localized bound states changes from four back to two as U is increased beyond the line AC. When U is increased further to cross the line OE, where the system enters zone-II(2), the characteristics of excitations with different spin-orientations are significantly different from each other, i.e., the shallow spin-up levels (solid lines) correspond to delocalized states, while the deep spin-down levels (dashed lines) still correspond to localized states, according to the spatial distribution of their wave functions. This feature of different localization for states with different spin orientations is due to the particularly strong splitting of the originally spin degenerated levels via the strong e-e interaction U, and brings about the complications for excitons in zone-II(2), mentioned above.

IV. RELAXATION PROCESS OF STE

In this section, we elucidate one of the important consequences of the emergence of new bound states due to the increase of the intrasite e-ph coupling λ_2, namely, the nonmonotonic dependence of lattice relaxation energy on λ_2, and then calculate the nonradiative transition rate under this circumstance.

A. Lattice relaxation energy

The lattice relaxation theory of multiphonon processes was developed in the early 1950s by Huang and Rhys[22] and others in connection with the radiative and nonradiative transitions of the F center. The difference in the lattice configurations of the initial and final electronic states gives rise to the multiphonon processes observed in experiments. This theory has been generalized by Su and Yu to consider localized excitations in quasi-one-dimensional systems, taking into account the self-consistency of the electronic states with lattice configurations.[23] A key quantity in this theory is the lattice relaxation energy E_r which in the present context can be written as (in units of t_0)

$$E_r = \frac{S\hbar\omega_b}{t_0} = \frac{1}{\pi\lambda_2}\sum_n |\gamma_n^i - \gamma_n^f|^2, \tag{4.1}$$

where γ_n^i and γ_n^f are dimensionless staggered lattice distortions in the initial and final states, respectively. The Huang-Rhys factor S is the average number of phonons (with energy $\hbar\omega_b$) emitted during the transition to bring the initial configuration into the final one.[23] In the nonradiative decay process, the initial state is the STE state, whereas the final one is the CDW ground state with constant γ_n^f. The curves of E_r and the energy difference between the initial and final states in the relaxation process of STE W_{if} as functions of λ_2 are plotted in Fig. 13. In this figure, as expected, W_{if} is a monotonically increasing function of λ_2. However, an abnormal behavior was found for the E_r curve. The lattice relaxation energy

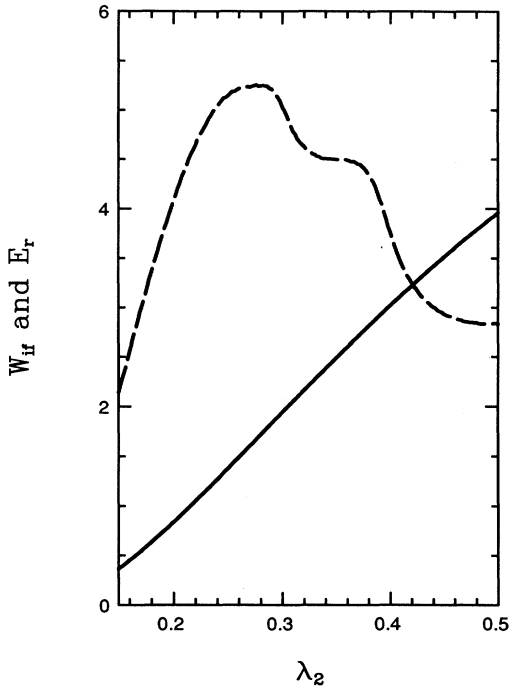

FIG. 13. The energy difference between the initial and the final states W_{if} (solid) and the lattice relaxation energy E_r (dashed) as functions of λ_2 for pure CDW STE, $N = 64$, $\lambda_1 = 0.0$, $U = V = 0.0$.

first increases in the small λ_2 region, and then decreases when λ_2 is greater than about 0.28.

This nonmonotonic feature can be qualitatively explained as follows: As seen from Eq. (4.1), the lattice relaxation energy is enhanced if the distortion increases or if the width of the distorted region increases. For weak coupling the increase of distortion dominates the decrease in extent, whereas for larger couplings both the distortion and the extent tend to their corresponding limiting values. In the strong coupling limit, i.e., as $\lambda_2 \to \infty$ ($t_0 \to 0$), E_r (in units of eV, while in this paper energies are measured in units of t_0) approaches the limiting value $3\beta^2/2K$.[8] These features can be qualitatively seen in Fig. 6 and have been checked by us numerically.

An amazing point is that this crossover from the weak-coupling behavior (where E_r increases with the increasing coupling strength) to the strong-coupling behavior (where E_r decreases and saturates with increased coupling) takes place exactly when new bound states are split off from the continuum. However, this is not so surprising because there are only two bound states for excitons in the weak-coupling continuum model, but four bound states in the strong-coupling limit.[8] Therefore, the crossover should show up as an appearance of new bound states inside the gap, giving rise to a downturn of the lattice relaxation energy. Since the nonradiative relaxation rate depends on E_r in an exponential way, this crossover is also the origin of the nonmonotonic behavior of the transition rate as we will see in the next subsection.

B. Nonradiative transition rate

Using the lattice relaxation formalism applied to quasi-one-dimensional systems, the nonradiative transition rate in the low temperature limit is written as[23]

$$W = \sqrt{\frac{2\pi}{\hbar\omega_b W_{if}}} \left(\frac{S}{p}\right)^p e^{(p-S)} \times \left[\frac{1}{4\hbar} G_1 \left(1 - \frac{p}{S}\right)^2 + \frac{1}{2\omega_b} G_2 \frac{p}{S}\right], \quad (4.2)$$

where $p = W_{if}/(\hbar\omega_b)$, and G_1 and G_2 are electronic matrix elements. These matrix elements depend on the overlap integral which is sensitive to the presence of new bound states. The detailed derivation is given in Appendix A.

The multielectron overlap integral $\langle e_f | e_i \rangle$ is related to the configurations of the initial and the final states. Since these states correspond to different lattice configurations, the overlap integral in general is not vanishing. Put another way, they belong to different complete sets, or different Hilbert spaces, if the system is infinite. The calculation of these multielectron overlap integrals is described in Appendix B. It is also noticed that the overlap integral has a general increasing tendency with the increase of the coupling strength. This increasing feature is due to the appearance of new bound states as well. In fact, according to the Levinson theorem,[17] the number of bound states split off from, say, the valence band is the difference of the phase shifts at the top and at the bottom of the band, divided by π. The new bound state split off from the valence band will cause the whole continuum to rearrange. Since the phase shift is defined up to modulo 2π, the difference of phase shifts is getting smaller when the number of bound states split off from a given band increases from one to two, resulting in an increase of the overlap integral.

Considering all the factors analyzed above, it is not difficult to understand the nonmonotonic behavior of the nonradiative transition probability curve (in the logarithmic scale) plotted in Fig. 14. There we plot $\log_{10} W$ vs λ_2 curve. As seen from Eq. (4.2), W depends not only on the dimensionless parameter λ_2, i.e., for a fixed λ_2 different combinations of t_0, β, and K will produce different W. Therefore we have fixed $t_0 = 0.7$ eV, $K = 6.16$ eV/Å, and mass of X ion $m = 35.4$ a.u. and let λ_2 vary with β in plotting Fig. 14. The shoulders in the curve are caused by the overlap integral $\langle e_i | e_f \rangle$, which takes very small values when the initial and final states are nearly orthogonal to each other for certain values of λ_2. The exact meaning of such a quasiorthogonality deserves further study .

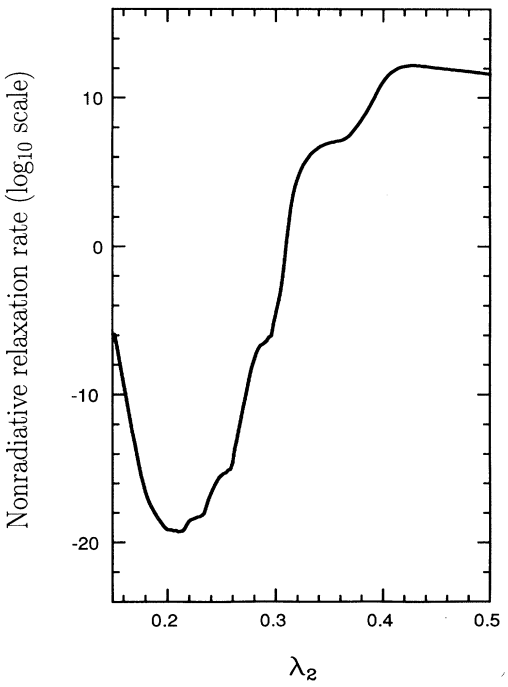

FIG. 14. The nonradiative relaxation rate as a function of λ_2. $N = 64$, $\lambda_1 = 0.0$, $U = V = 0$, $t_0 = 0.7$ eV, $K = 6.16$ eV/Å, and $m = 35.4$ a.u. Only β varies with λ_2.

V. CONCLUSIONS AND DISCUSSIONS

In this last section, we discuss the connections between our numerical results and experimental investigations and make some concluding remarks.

As described in the above sections, within the Hartree-Fock approximation, the properties of the homogeneous ground state have been studied as a function of the Coulomb on-site interaction U and intrasite e-ph coupling strength λ_2. We found that for a variety of physical parameters of real MX-chain materials, the ground state is the CDW state with Peierls instability when U is relatively small and λ_2 is relatively large, while the SDW state with vanishing lattice distortions prevails in the opposite limit. For a particular material, the x-ray diffraction and elastic neutron scattering experiments can be used to determine whether the ground state is CDW or not, whereas the neutron scattering and the spin resonance experiments such as EPR or NMR can be used to check whether SDW is the ground state. There is some consensus now among the researchers that PtCl is a strongly distorted CDW material, and NiBr is a SDW system without lattice distortion, while PtI is an in-between CDW system with very small distortion. It is also noticed that some new aspects of the Peierls instability (e.g., spin-Peierls) will show up as the temperature is different from zero because of the particularly strong competition of the CDW and SDW in the intermediate region of our phase diagram. It is expected that the temperature dependence of some observations will be modified by this competition, which will guide our further investigations.

Evidence for the locally inhomogeneous excitations in MX-chain materials has been provided by several experimental probes, such as resonance Raman spectra,[20] polarized reflection and luminescence,[21] photo-induced

absorption,[24] which also indicated at the non-negligible role of Coulomb interactions for these materials. According to our calculations presented above, the STE in the CDW dominating regime always contains locally nonvanishing SDW distortions, and even in a part of SDW dominating regime [zone-II(1) in Fig. 1], the STE and polarons are still accompanied by local nonvanishing CDW distortions. Therefore, electron-nuclear-double-resonance (ENDOR) experiments can be suggested to verify this particular feature, because the double resonance of a microwave and a radiofrequency field can give information of local hyperfine interactions directly, which can be used to determine the site-dependent spin density except for the sign. Moreover, electron-nuclear-nuclear-triple-spin-resonance (TRIPLE) measurements with a third resonance with an additional radiofrequency field can provide information about the fine structure of each type of STE and polarons with different symmetries described above, including the sign of spin.[25] It would be interesting to check our theoretical predictions in such experiments.

In addition, we have also shown that the number of localized bound states in exciton and polaron channels changes from two to four, and from two to three, respectively, as the e-ph coupling strength λ_2 is increased across the curve AC in Fig. 1, which has some important physical consequences. The nonradiative transitions of these localized excitations have been studied with the conclusion that the crossover from the weak-coupling to strong-coupling behavior showing up as emergence of new bound states inside the gap is the origin of the nonmonotonic behavior of the lattice relaxation energy, which in turn explains the nonmonotonic behavior of the transition rate. In this connection we note that the time-resolved photoluminescence (PL) measurements[26] yield very short lifetime of the order of 100 ps for STE in PtCl samples. If we adopt the parameters suggested in Ref. 27 $K = 6.16$ eV/Å^2, $\beta = 2.36$ eV/Å, $t_0 = 0.7$ eV, $\lambda_2 = 0.41$, $\hbar\omega_b = 0.038$ eV, the nonradiative decay rate of STE is calculated to be $6.7 \times 10^{11}\text{sec}^{-1}$, i.e., even larger than the observed value. Very interesting results on PL of mixed crystals $PtCl_{1-x}Br_x$ were reported in Ref. 28. It has been observed that the linewidth of PL almost does not change with x, while one would expect broadening in the middle range of mixing because STE on Br and Cl to be quite different. On the other hand, the intensity of PL drops by a factor of 100 when x increases from 0 to 1. It seems to us that a natural explanation would be that the PL is mainly coming from Cl but not from Br. This would happen if we assume that parameters for Br correspond to the transition region with higher relaxation rate. Of course, further theoretical and experimental work (such as photoinduced absorption in an infrared region) is needed to confirm this interpretation. We should, however, mention that this assumption is also consistent with the resonance Raman data,[29] namely, the intensity and number of satellite lines are much bigger for Cl than for the Br case. The theoretical calculations of the optical absorption based on the lattice relaxation approach are in progress, which can also include the nonlinear dynamical process of the lattice neglected in the current investigation.

In most calculations reported above, the intersite e-ph coupling λ_1 and the nearest-neighbor Coulomb interaction V have not been included. Generally, the effect of the λ_1 term is to produce the BOW order in the ground state, and to provide another channel for the locally inhomogeneous excitations in addition to the CDW channel produced by the λ_2 term. Although the simultaneous competitions of BOW, CDW, and SDW can bring about some complications in the phase diagram if the effect of λ_1 is taken into account, it is still reasonable to believe that the main results about the existence of the localized nonvanishing SDW (or CDW) distortions and the nonmonotonic dependence of the relaxation rate on the coupling constant due to the emergence of new localized bound states will not be changed qualitatively. However, the possibility of coexistence of SDW, CDW, and BOW would appear as a result of including the λ_1 term, and some new features would also be expected for the localized excitations. For example, the spin-Peierls phase with coexistence of CDW and SDW will emerge directly as a result of including the λ_1 term, which has been found by the Los Alamos group with a quantum variational calculation.[10] Another example is the emergence of irrationally charged solitons in the possible coexistence region.[30] On the other hand, the next neighbor Coulomb interaction V generally favors the CDW state, and leads to splitting of singlet and triplet excitons related to Coulomb binding. This effect has not been considered in the above calculations. We have indications that the effect of V on the localized excitations is not crucial, mainly because of the smallness of V compared with U and t_0 which is true for a wide variety of materials. Furthermore, the correlation effects due to Coulomb interactions between electrons, which have been neglected in this Hartree-Fock framework, should be considered to clarify which of the three main orders (BOW, CDW, and SDW) is favored for various MX materials.[10,31]

The one-band model in our consideration does not take the effects of electrons on the X ions explicitly into account under the assumption that the difference of the on-site affinities on the M and X ions is much larger than the bandwidth. But when the system is in the weak coupling limit, the strong hybridization between electrons on M ions and on X ions will play an important role in determining the properties of the system. In that case the two-band model should be employed and some two-band features will appear, such as the asymmetry of the positively and negatively charged excitations and the long period superlattice structures in the strongly hybridized case.[10] Of course,we cannot detect these features in our one-band calculations, but it is reasonable to believe that for a large variety of MX materials, the main effects we considered in the above sections within the one-band model will survive the two-band complications and can be checked directly by experiments.

In conclusion, within the BdeG formalism for the 1D single-band Peierls-Hubbard model, the localized excitations (STE and polarons) in the quasi-one-dimensional systems like MX chains have been extensively investigated under the BOW-CDW and CDW-SDW competitions. The profiles of these nonlinear excitations have

been elaborated in a wide parameter scope of the driving e-ph and e-e interactions to cope with the well-known tunability of the MX-chain family. The corresponding coexistence of local BOW, CDW, and SDW distortions is demonstrated, and two different types of STE with different patterns of CDW-SDW distortions and charge transfer are found as the on-site e-ph coupling λ_2 increases above or the e-e interaction U decreases below a well-defined boundary in the parameter space. These theoretical predictions are suggested for experimental verification using ENDOR and TRIPLE techniques. As another effect of the increase of λ_2, the number of bound states inside the gap is found to change from two to four for the STE case and from two to three for the polaron case, which could also be verified in optical experiments. Within the lattice relaxation approach, the nonmonotonic dependence of the lattice relaxation rate on λ_2 is manifested as a consequence of the crossover from the weak-coupling to strong-coupling bahavior signaled by the emergence of new bound states, and is used to tentatively interpret the very short lifetime of STE in PtCl complexes.

It seems to us that the peculiar features found in our studies of the Peiers-Hubbard model, namely, the crossover from the weak-coupling to strong-coupling behavior as the new bound states emerge in the gap, the nonmonotonic dependence of the relaxation rate upon the coupling constant, and the pattern change of localized excitations, might be more generic in quasi-one-dimensional systems with competing interactions. They certainly deserve further experimental and theoretical exploration.

ACKNOWLEDGMENTS

One of us (L.Y.) would like to thank A. R. Bishop for helpful discussions. W.Z.W. would like to thank the ICTP for the hospitality under the Federation Scheme and Dr. J. B. Wu for helpful discussions. This work was partly supported by the National Natural Science Foundation of China.

APPENDIX A: FORMALISM FOR CALCULATING THE NONRADIATIVE TRANSITION RATE

We start from the original Hamiltonian, Eq. (2.1), to calculate the nonradiative transition probabilities. The phonon part of the Hamiltonian should be normalized as

$$\frac{K}{2}\sum_n\left[(u_n-v_n)^2+(u_n-v_{n+1})^2\right]=\frac{1}{2}\sum_{q\,l}\omega_{q\,l}^2 Q_{q\,l}^* Q_{q\,l}\ , \tag{A1}$$

where $Q_{q\,l}$ are normal coordinates, $\omega_{q\,l}$ are phonon frequencies, q is the wave vector, and l is the phonon branch index.

After dimerization, each cell contains four atoms, two M atoms and two X atoms, so we have four branches of phonons. Adding the kinetic energy of phonons to the original Hamiltonian, having the phonon part second quantized, the total Hamiltonian can be rewritten as[23]

$$\begin{aligned}
&\mathcal{H}=\mathcal{H}_0^e+\mathcal{H}_0^{\rm ph}+\mathcal{H}_{\rm int}\ ,\\
&\mathcal{H}_0^e=H_0+\sum_{q\,l}S_{q\,l}Q_{q\,l}^c+\frac{1}{2}\sum_{q\,l}\omega_{q\,l}^2 Q_{q\,l}^{c\,*}Q_{q\,l}^c\ ,\\
&\mathcal{H}_0^{\rm ph}=\frac{1}{2}\sum_{q\,l}\hat{P}_{q\,l}^\dagger\hat{P}_{q\,l}+\frac{1}{2}\sum_{q\,l}\omega_{q\,l}^2(\widehat{Q}_{q\,l}-Q_{q\,l}^c)^\dagger \\
&\qquad\qquad\times(\widehat{Q}_{q\,l}-Q_{q\,l}^c)\ ,\\
&\mathcal{H}_{\rm int}=\sum_{q\,l}(S_{q\,l}+\omega_{q\,l}Q_{q\,l}^{c\,*})(\widehat{Q}_{q\,l}-Q_{q\,l}^c)\ ,
\end{aligned} \tag{A2}$$

where

$$H_0=-\sum_{i\,s}t_0(c_{2i+1\,s}^\dagger c_{2i\,s}+c_{2i\,s}^\dagger c_{2i-1\,s}+\text{H.c.})+\text{Hubbard terms.}$$

and

$$S_{q\,l}=\frac{1}{\sqrt{N}}\sum_{i\,\lambda}\sum_s S_{i\lambda,s}\frac{1}{\sqrt{m_\lambda}}\varepsilon_\lambda(l,q)e^{iqR_i}\ . \tag{A3}$$

Here i is the cell index, s is the spin index, and λ accounts for the atoms within one cell. R_i is the cell coordinate, N is the total number of cells. $m_1=m_2$ is the mass for the metal atoms whereas $m_3=m_4$ is the mass for the halogen atoms. $\widehat{Q}_{q\,l}$ are the normal phonon operators. $\varepsilon_\lambda(l,q)$ are phonon normal modes which obey the orthogonality relations

$$\begin{aligned}
&\sum_l\varepsilon_{\lambda'}^*(l,q)\varepsilon_\lambda(l,q)=\delta_{\lambda'\lambda}\ ,\\
&\sum_\lambda\varepsilon_\lambda^*(l',q)\varepsilon_\lambda(l,q)=\delta_{l'l}\ .
\end{aligned} \tag{A4}$$

The electronic operators $S_{i\lambda,s}$ in Eq. (A3) are defined as

$$\begin{aligned}
S_{i1,s}&=-\alpha(c_{2i\,s}^\dagger c_{2i-1\,s}-c_{2i-1\,s}^\dagger c_{2i-2\,s}+\text{H.c.})\ ,\\
S_{i2,s}&=-\alpha(c_{2i+1\,s}^\dagger c_{2i\,s}-c_{2i\,s}^\dagger c_{2i-1\,s}+\text{H.c.})\ ,\\
S_{i3,s}&=\beta(c_{2i-1\,s}^\dagger c_{2i-1\,s}-c_{2i-2\,s}^\dagger c_{2i-2\,s}+\text{H.c.})\ ,\\
S_{i4,s}&=\beta(c_{2i\,s}^\dagger c_{2i\,s}-c_{2i-1\,s}^\dagger c_{2i-1\,s}+\text{H.c.})\ .
\end{aligned} \tag{A5}$$

One can see from the rearranged Hamiltonian (A2) that all terms having factors $Q_{q\,l}^c$ exactly cancel each other, and we can recover the original Hamiltonian. Therefore, we can choose as $Q_{q\,l}^c$ either the initial state lattice configuration or the final state lattice configuration. The most important thing is that the electronic state $|e\rangle$ and the phonon state $|\tilde{n}\rangle$ each of which depends on the lattice configuration and diagonalizes the noninteracting $\mathcal{H}_0^e$ and $\mathcal{H}_0^{\rm ph}$, respectively, should be chosen such that the following equations are valid:

$$\begin{aligned}
&\langle e|\mathcal{H}_{\rm int}|e\rangle=0,\\
&\langle\tilde{n}|\mathcal{H}_{\rm int}|\tilde{n}\rangle=0.
\end{aligned} \tag{A6}$$

The former equation leads to the gap equation, whereas the latter provides the definition of Q^c_{ql},

$$Q^c_{ql} = \langle\tilde{n}|\hat{Q}_{ql}|\tilde{n}\rangle \quad , \tag{A7}$$

representing the dynamical symmetry breaking. The initial state $|i\rangle$ is represented as $|i\rangle = |e_i\rangle \bigotimes |\tilde{n}_i\rangle$, whereas the final state is represented as $|f\rangle = |e_f\rangle \bigotimes |\tilde{n}_f\rangle$. For the initial state, Q^c_{ql} should be replaced by Q^i_{ql}, and for the final state, Q^c_{ql} should be replaced by Q^f_{ql}. Therefore, the Hamiltonian in Eq. (A6) can be split in two ways, one using the initial lattice configuration, the other using the final lattice configuration, and they should be equivalent to each other.

Within the lattice relaxation formalism applied to quasi-one-dimensional systems, developed by Su and Yu, the nonradiative transition probability in the Born approximation is given by[23]

$$W = \frac{2\pi}{\hbar}\mathcal{A}^v_i \sum_f |\langle f|\mathcal{H}_{\rm int}|i\rangle|^2 \delta\Bigg(W_{if} + \sum_q (n^i_q + \tfrac{1}{2})\hbar\omega_q - \sum_q (n^f_q + \frac{1}{2})\hbar\omega_q\Bigg) \, , \tag{A8}$$

where $\mathcal{A}^v_i$ means statistical average over the initial states and a summation over the required final state is understood. The energy difference W_{if} between the initial and final states is expressed as

$$W_{if} = \sum_{k_i}\epsilon_{k_i} - \sum_{k_f}\epsilon_{k_f} + \frac{1}{2}\sum_{ql} {Q^i_{ql}}^* Q^i_{ql} - \frac{1}{2}\sum_{ql} {Q^f_{ql}}^* Q^f_{ql} \quad , \tag{A9}$$

where the letters i, f indicate the initial or final states, respectively, and the summations $\sum_{k_i}$ and $\sum_{k_f}$ are carried over all occupied single electron states.

In accordance with the previous discussion, either $\mathcal{H}^i_{\rm int}$ for the initial state or $\mathcal{H}^f_{\rm int}$ for the final state can be used here to calculate the matrix element in Eq. (A8). The results should be identical since, according to the general theory of quantum transition, the transition probability does not depend on the way the total Hamiltonian is split, provided the total energy is conserved. Hereafter, we use $\mathcal{H}^i_{\rm int}$ in the numerical calculation, and also omit the BOW part of $\mathcal{H}^i_{\rm int}$, namely, set $\alpha = 0$.

By making use of the steepest descent method and taking low temperature limit, the nonradiative transition probability can be explicitly calculated to yield

$$W = \sqrt{\frac{2\pi}{\hbar\omega_b W_{if}}}\left(\frac{S}{p}\right)^p e^{(p-S)} \times \left(\frac{1}{4\hbar}G_1\left[1-\frac{p}{S}\right]^2 + \frac{1}{2\omega_b}G_2\frac{p}{S}\right] \quad , \tag{A10}$$

where $p = W_{if}/\hbar\omega_b$; G_1 and G_2 are electronic matrix elements,

$$G_1 = \left|\sum_n (S_n + m\omega_b^2\langle e_i|e_f\rangle v^i_n)(v^f_n - v^i_n)\right|^2 \quad ,$$
$$G_2 = \frac{1}{m}\sum_n |S_n + m\omega_b^2\langle e_i|e_f\rangle v^i_n|^2 \, , \tag{A11}$$

with n as the index of the metallic sites, while the calculation of the overlap integral $\langle e_i|e_f\rangle$ and the matrix element S_n will be given in Appendix B.

APPENDIX B: THE MULTIELECTRON MATRIX ELEMENTS

The electron overlap integral $\langle e_i|e_f\rangle$ is a product of two $\frac{N}{2}$ by $\frac{N}{2}$ Slater determinants, $\langle e_i|e_f\rangle_\downarrow$ and $\langle e_i|e_f\rangle_\uparrow$, where $\frac{N}{2}$ is the number of electrons for each spin orientation in the system. For simplicity, in the original paper of Su and Yu,[23] a Hartree approximation was used to calculate the matrix elements. Later on, Gu and Wang[32] did the calculation with Slater determinants. Their results are outlined here for the convenience of reference.

Suppose in the initial state an electron with spin $\uparrow$ is photogenerated, then the system approaches the final state, i.e., the ground state, via a nonradiative transition. We have the following explicit form of $\langle e_i|e_f\rangle$

$$\langle e_i|e_f\rangle = \langle e_i|e_f\rangle_\downarrow \langle e_i|e_f\rangle_\uparrow = \begin{Vmatrix} \langle\bar{1}|1\rangle_\downarrow & \cdots & \langle\bar{1}|\frac{N}{2}\rangle_\downarrow \\ \cdots & \cdots & \cdots \\ \langle\overline{\frac{N}{2}-1}|1\rangle_\downarrow & \cdots & \langle\overline{\frac{N}{2}-1}|\frac{N}{2}\rangle_\downarrow \\ \langle\frac{N}{2}|1\rangle_\downarrow & \cdots & \langle\frac{N}{2}|\frac{N}{2}\rangle_\downarrow \end{Vmatrix} \begin{Vmatrix} \langle\bar{1}|1\rangle_\uparrow & \cdots & \langle\bar{1}|\frac{N}{2}\rangle_\uparrow \\ \cdots & \cdots & \cdots \\ \langle\overline{\frac{N}{2}-1}|1\rangle_\uparrow & \cdots & \langle\overline{\frac{N}{2}-1}|\frac{N}{2}\rangle_\uparrow \\ \langle\overline{\frac{N}{2}+1}|1\rangle_\uparrow & \cdots & \langle\overline{\frac{N}{2}+1}|\frac{N}{2}\rangle_\uparrow \end{Vmatrix} \quad , \tag{B1}$$

where $|\bar{k}_i\rangle$ and $|k_f\rangle$ represent the molecular orbitals for the initial and final configurations, respectively. Here we label the molecular orbital levels up from the bottom of the valence band, and

$$\langle\bar{k}_i|k_f\rangle_s = \sum_{n=1}^{N} \bar{\psi}^*_{k_i s}(n)\psi_{k_f s}(n) \quad .$$

The matrix elements in Eq. (A11) are given as

$$S_n = \beta\sum_s \langle e_i|(c^\dagger_{n\,s}c_{n\,s} - c^\dagger_{n-1\,s}c_{n-1\,s})\,|e_f\rangle \quad , \tag{B2}$$

which can be defactorized as

$$S_n = \langle e_i|e_f\rangle_\uparrow S_{n\downarrow} + \langle e_i|e_f\rangle_\downarrow S_{n\uparrow}$$

with

$$S_{n\,s} = \beta\langle e_i|(c^{\dagger}_{n\,s}c_{n\,s} - c^{\dagger}_{n-1\,s}c_{n-1\,s})|e_f\rangle_s \ ,$$

where $S_{n\,s}$ is a sum of $\frac{N}{2}$ Slater determinants of $\frac{N}{2}$ by $\frac{N}{2}$. The k_fth determinant of $\langle e_i|c^{\dagger}_{n\,s}c_{n\,s}|e_f\rangle_s$ $(k_f = 1, ..., \frac{N}{2})$, is a determinant of $\langle e_i|e_f\rangle_s$ with its k_fth column being replaced by a column vector $\bar{\psi}^*_{k_i}(n)\psi_{k_f}(n)$ $(k_i = 1, \ldots, \frac{N}{2} - 1, \frac{N}{2}+1)$ for spin $\uparrow$ and $(k_i = 1, ..., \frac{N}{2})$ for spin $\downarrow$, i.e.,

$$\langle e_i|c^{\dagger}_{n\uparrow}c_{n\uparrow}|e_f\rangle = \langle e_i|e_f\rangle_{\downarrow}\langle 0| \times \prod_{k_i=1}^{\frac{N}{2}} \bar{c}_{k_i\uparrow}(c^{\dagger}_{n\uparrow}c_{n\uparrow}) \prod_{k_f=1}^{\frac{N}{2}} c^{\dagger}_{k_f\uparrow}|0\rangle \tag{B3}$$

with

$$\begin{aligned}
&\langle 0| \prod_{k_i=1}^{\frac{N}{2}} \bar{c}_{k_i\uparrow}(c^{\dagger}_{n\uparrow}c_{n\uparrow}) \prod_{k_f=1}^{\frac{N}{2}} c^{\dagger}_{k_f\uparrow}|0\rangle \\
&= \begin{Vmatrix} \bar{\psi}^*_1(n)\psi_1(n) & \langle\overline{1}|2\rangle & \cdots & \langle\overline{1}|\frac{N}{2}\rangle \\ \cdots & \cdots & \cdots & \cdots \\ \bar{\psi}^*_{\frac{N}{2}-1}(n)\psi_1(n) & \langle\overline{\frac{N}{2}-1}|2\rangle & \cdots & \langle\overline{\frac{N}{2}-1}|\frac{N}{2}\rangle \\ \bar{\psi}^*_{\frac{N}{2}+1}(n)\psi_1(n) & \langle\overline{\frac{N}{2}+1}|2\rangle & \cdots & \langle\overline{\frac{N}{2}+1}|\frac{N}{2}\rangle \end{Vmatrix} + \begin{Vmatrix} \langle\overline{1}|1\rangle & \bar{\psi}^*_1(n)\psi_2(n) & \cdots & \langle\overline{1}|\frac{N}{2}\rangle \\ \cdots & \cdots & \cdots & \cdots \\ \langle\overline{\frac{N}{2}-1}|1\rangle & \bar{\psi}^*_{\frac{N}{2}-1}(n)\psi_2(n) & \cdots & \langle\overline{\frac{N}{2}-1}|\frac{N}{2}\rangle \\ \langle\overline{\frac{N}{2}+1}|1\rangle & \bar{\psi}^*_{\frac{N}{2}+1}(n)\psi_2(n) & \cdots & \langle\overline{\frac{N}{2}+1}|\frac{N}{2}\rangle \end{Vmatrix} \\
&+ \cdots + \begin{Vmatrix} \langle\overline{1}|1\rangle & \cdots & \langle\overline{1}|\frac{N}{2}-1\rangle & \bar{\psi}^*_1(n)\psi_{\frac{N}{2}}(n) \\ \cdots & \cdots & \cdots & \cdots \\ \langle\overline{\frac{N}{2}-1}|1\rangle & \cdots & \langle\overline{\frac{N}{2}-1}|\frac{N}{2}-1\rangle & \bar{\psi}^*_{\frac{N}{2}-1}(n)\psi_{\frac{N}{2}}(n) \\ \langle\overline{\frac{N}{2}+1}|1\rangle & \cdots & \langle\overline{\frac{N}{2}+1}|\frac{N}{2}-1\rangle & \bar{\psi}^*_{\frac{N}{2}+1}(n)\psi_{\frac{N}{2}}(n) \end{Vmatrix} \ .
\end{aligned} \tag{B4}$$

There are $\frac{N}{2}$ terms in the right hand side of the above equation. It is noted that the steepest descent approximation is valid only if the following inequality is held:

$$\left|\frac{W_{if} - S\langle\hbar\omega\rangle}{S\langle\hbar\omega\rangle}\right| \lesssim 1 \ .$$

This inequality may be roughly interpreted as the smallness of the difference for W_{if} and lattice relaxation energy compared with the lattice relaxation energy itself.

*Present address: Department of Physics, University of Arizona, Tucson, AZ 85721

[1] See, e.g., P. Day, in *Low-Dimensional Cooperative Phenomena*, edited by H. J. Keller (Plenum, New York, 1974), p. 191; H. J. Keller, in *Extended Linear Chain Compounds*, edited by J. S. Miller (Plemum, New York, 1982), Vol. 1, p. 357.

[2] See R. J. H. Clark, in *Advances in Infrared and Raman Spectroscopy*, edited by R. J. H. Clark and R. E. Hester (Wiley, New York, 1984), Vol. 22, p. 95.

[3] See, *e.g.*, Synth. Met. **29**, F123 (1989); **41-43**, 2715 (1991); **55-57**, 3329 (1993).

[4] K. Nasu, J. Phys. Soc. Jpn. **50**, 235 (1981); **52**, 3865 (1983); **53**, 302 (1984) **53**, 427 (1984); **54**, 1933 (1985); J. Lumin. **38**, 90 (1987).

[5] W. P. Su, J. R. Schrieffer, and A. J. Heeger, Phys. Rev. Lett. **42**, 1698 (1979); Phys. Rev. B **22**, 2209 (1980); **28**, 1138(E) (1983).

[6] S. Ichinose, Solid State Commun. **50**, 137 (1984).

[7] Y. Onodera, J. Phys. Soc. Jpn. **56**, 250 (1987).

[8] D. Baeriswyl and A. R. Bishop, Phys. Scr. **T 19**, 239 (1987); J. Phys C **21**, 399 (1988).

[9] A. R. Bishop, J. T. Gammel, and S. R. Phillpot, Synth. Met. **29**, F151 (1989).

[10] J. Tinka Gammel *et al.*, Phys. Rev. B **45**, 6408; S. M. Weber-Milbrot *et al., ibid.* **45**, 6435 (1992).

[11] See, e.g., R. C. Albers, Synth. Met. **29**, F169 (1989); M. Alouani *et al.*, Synth. Met. **55-57**, 3352 (1993).

[12] A. Painelli and A. Girlando, Phys. Rev. B **37**, 5748 (1988); **39**, 9663(E) (1989); Synth. Met. **29**, F181 (1989); **41-43**, 2721 (1991).

[13] See, e.g., D. Baeriswyl, D. K. Campbell, and S Mazumdar, in *Conjugated Conducting Polymers*, edited by H. Kiess (Springer, Berlin, 1992), p. 7.

[14] A. Mishima and K. Nasu, Phys. Rev. B **39**, 5758 (1989); **39**, 5763 (1989); **40**, 5593 (1989).

[15] J. Tinka Gammel *et al.*, Synth. Met. **55-57**, 3397 (1993).

[16] K. Yonemitsu, A.R. Bishop, and J. Lorenzana, Phys. Rev. B **45**, 8065 (1993).

[17] See, e.g., L. Yu, *Solitons and Polarons in Conducting Polymers* (World Scientific, Singapore, 1988).

[18] C. L. Wang, G. L. Gu, Z. B. Su, and L. Yu, Synth. Met. **29**, 3643 (1991); in *Electronic Properties of Polymers*, edited by M. Kuzmany, M. Mehring, and S. Roth (Springer-Verlag, Berlin, 1992), p. 72.

[19] W. Z. Wang, C. L. Wang, Z. B. Su, and L. Yu, Synth. Met. **55-57**, 3370 (1993).

[20] H. Tanino, K. Kobayashi, and T. Koda, Phys. Rev. B **52**,

1446 (1983).
[21]Y. Wada, T. Mitani, M. Yamashita, and T. Kota, J. Phys. Soc. Jpn. **54**, 3143 (1985).
[22]K. Huang and A. Rhys, Proc. Soc. (London) Ser. A **204**, 406 (1950).
[23]Z. B. Su and L. Yu, Phys. Rev. B **27**, 5199 (1983); **B29**, 2309(E) (1984); Commun. Theor. Phys. **2**, 1203(1983); **2**, 1323 (1983); **2**, 1341 (1983).
[24]S. Kurita, M. Haruki, and K. Miyagawa, J. Phys. Soc. Jpn. **57**, 1789 (1989).
[25]H. Thomann and L. R. Dalton, in *Handbook of Conducting Polymers*, edited by T. A. Skotheim (Dekker, New York, 1986), Vols. 1 and 2, p. 1157.
[26]H. Tanino, W. W. Rühle, and K. Takahashi, Phys. Rev. **B 38**, 12 716 (1988); Y. Wada, K. Era, and M. Yamashita, Solid State Commun. **67**, 953 (1988).
[27]L. Degiorgi, P. Wachter, M. Haruki, and S. Kurita, Phys. Rev. B **40**, 3285 (1989).
[28]H. Tanino, W. W. Rühle, and K. Takahashi, Phys. Rev. **B 38**, 12 716 (1988); H. Tanino *et al.*, Synth. Met. **41-43**, 2797 (1991).
[29]B. Swanson *et al.*, Synth. Met. **41-43**, 2733 (1991).
[30]S. Kivelson, Phys. Rev. B **28**, 2653 (1983).
[31]S. Kivelson and D. E. Heim, Phys. Rev. B **26**, 4278 (1982).
[32]Z.Q. Gu and Y.L. Wang, Chin. J. Semicond. **5**, 585 (1984).